# Design and Projected Performance of a Flapping Foil AUV

Stephen Licht, Victor Polidoro, Melissa Flores, Franz Hover, and Michael Triantafyllou
Department of Ocean Engineering
Massachusetts Institute of Technology
Cambridge, MA 02134
Email: slicht@mit.edu

***Abstract*— The design and construction of a Biomimetic Flapping Foil AUV is detailed. The vehicle was designed as a proof of concept for the use of oscillating foils as the sole source of motive power for a cruising and hovering underwater vehicle. Primary vehicle design requirements included scalability and flexibility in terms of the number and placement of foils, so as to maximize experimental functionality. This goal was met by designing an independent, self-contained module to house each foil, requiring only 24V DC power and a connection to the vehicle's Ethernet LAN for operation. All other vehicle components are contained in housings which can be repositioned to any point on the central aluminum spine that comprises the vehicle frame.**

**The results of tests on the foil modules in the MIT Marine Hydrodynamics Water Tunnel and MIT Ship Model Testing Tank are used both to demonstrate fundamental properties of flapping foils, and to predict the performance of the specific vehicle design based on the limits of the actuators. The maximum speed of the vehicle is estimated based on the limitations of the specific actuator, and is shown to be a strong function of the vehicle drag coefficient. When using four foils, the maximum speed increases from 1m/s with a vehicle $C_D$ of 1.4 to 2m/s when $C_D = 0.1$, where $C_D$ is based on vehicle frontal area.**

**Finally, issues of vehicle control are considered, including the decoupling of speed and pitch control using pitch biased maneuvering, and the trade-off between actuator bandwidth and authority both during cruising and hovering operation.**

## I. Introduction

The physics of swimming and flying has been the focus of considerable theoretical, numerical and experimental work (see, for example, [1], [2], [3], [4], [5], [6].) One of the motivations has been to improve the design and performance of underwater vehicles, recognizing that in many ways there is an extraordinary gap between the abilities of man-made machines and those of fish and other marine animals. Existing AUVs are typically optimized primarily for high cruising efficiency with propellers and conventional lifting surfaces, and as a result are unsuited for use in confined spaces, at low speeds, near the surface, and in unsteady flow, conditions where fish can thrive. A robust vehicle that exploits the hydrodynamics of fishlike swimming could yield impressive gains in maneuvering and hovering capabilities while maintaining the ability to cruise from station to station with high efficiency. Such a vehicle could serve as an extremely powerful tool in a wide range of applications.

The BFFAUV was conceived as a test platform and proof of concept for the use of flapping foils as the sole source of propulsion and maneuvering forces in an underwater vehicle. Extensive testing of oscillating foils has been performed in the MIT Ship Model Testing Tank, resulting in a solid understanding of the fundamental parameters of thrust production in foils [7], [8], [9]. The BFFAUV represents a first attempt to tackle the issues involved in putting this knowledge into practice on a working vehicle. The focus of the design has been on those issues which are related specifically to the the foils themselves. As a result, there was no allowance made for a mission payload, and vehicle size, shape and control systems were designed to be as flexible as possible.

Knowledge gained from the major problems in the mechanics and controls of this vehicle should help guide future hydrodynamic research and suggest ways to maximize the performance and minimize the complexity of flapping foil propulsion.

## II. Vehicle Requirements

The vehicle design specifications can be separated into performance goals and functional requirements. Performance goals are overall goals for the vehicle which do not explicitly impose constraints on the design itself, such as desired maximum speed and maneuvering capabilities. Functional requirements stem both from the performance goals and from the experimental rationale for the project, e.g. mandating the use of flapping foils.

The performance goals for the vehicle include a desired top speed of 2m/s and sufficient maneuvering authority to independently control position in pitch, heave, surge and sway. Functional requirements include

- Foil based actuation - the primary goal of the program is to investigate the use of foils for propulsion and maneuvering.
- Scalability and flexibility - freedom to adjust foil actuator numbers, positions and orientations will allow insights into the tradeoffs between different vehicle layouts and the corresponding control strategies.
- Size constraints - 2m x 0.5m x 0.5m maximum dimensions will make deployment problems in the MIT Towing Tank, swimming pools and the Charles River tractable.
- Autonomous operation - pre-programmed mission following, independent error handing, onboard power source, and data storage capability.

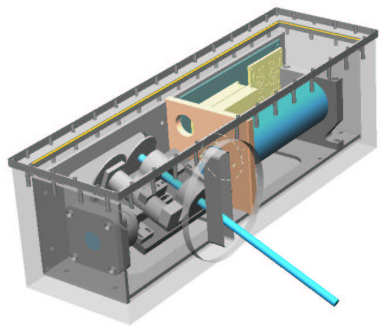

Fig. 1. Single Housing Actuator Design

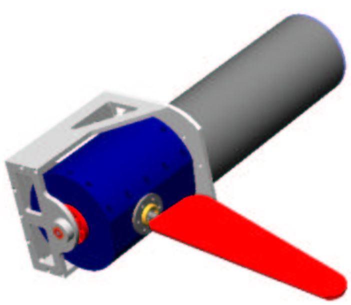

Fig. 2. Dual Housing Actuator Design

- Shallow (10m), confined water operation - a greater depth rating adds cost and complexity with no corresponding increase in experimental functionality.
- Inertial navigation - minimal long term tracking accuracy is required for short, supervised missions focused on local control issues.

## III. Vehicle Design

### A. Foil Actuators

The focus of much of the design effort for the vehicle was concentrated on the distinguishing characteristic of the vehicle, the foil actuation. A key requirement for the vehicle was scalability and flexibility in terms of the number of foils, as well as their positions and orientations. To meet the flexibility requirement, each foil actuator was conceived as part of a waterproof module that could be mounted anywhere on the vehicle frame, and be operated independently from the other foils. To allow for scalability, the modules are designed such that as more modules are added to the vehicle, there is no complexity added to the power and communication circuits.

A single foil module contains all the components necessary to add another foil to the vehicle. Each module contains a 196W and a 15W DC brush motor with optical encoders (Litton-Polyscientific, Blacksburg, VA) which actuate foil roll and pitch, respectively. The corresponding motor control circuit is also housed in the module, with an Ethernet enabled 2-axis motion control card, and two PWM amplifiers. The addition of a new module entails only two connections: an Ethernet line to a central hub on the vehicle LAN, and a fused connection to the power bus. Since the hub acts in some sense like a bus connection, no additional wiring is required.

There are two generations of foil actuator designs. In the first design, all the components were placed in a single housing, as drawn in Figure 1. While the mechanical actuation and internal wiring was straightforward within the single housing, the sealing was complex. The dynamic seal between the foil and the housing limited the depth of operation, range of motion, and the fatigue lifetime. After construction of a prototype, a second iteration was proposed to increase the depth rating of the actuator and the range of roll motion of the foil. The first prototype was installed in the MIT Propeller Testing Tunnel for experiments as described below.

The second iteration of the design, which is currently installed on the vehicle, contains the same electrical components in two independently sealed cylindrical housings, as shown in Figure 2. One cylinder remains stationary with respect to the vehicle and the second, smaller cylinder rotates about its axis with respect to the larger. The use of two independently rotating housings simplified the sealing problem, which improved the robustness of the seals. In addition, the full range of motion on the roll axis was improved to $180°$, while the pitch motion remains completely unrestricted.

In order to maximize the reliability, and hence the usefulness of the vehicle as a platform for different research teams, an emphasis was placed on simplicity and robustness of the actuators. One result is that mass of the solid moving parts in the dual housing design is relatively high, increasing the energy wasted on overcoming the rotational inertia, and potentially decreasing the bandwidth of thrust vectoring. We anticipate that future designs can be made substantially smaller and lighter, once testing and long term operation reveal areas of over- and under-design. In addition, once minimizing module size becomes a priority, e.g. with the need for payload space and reduced power operation, the cost of smaller components will become justified.

### B. Other Vehicle Design Details

The power system is run at 24V DC for reasons of safety and convenience, supplied by a pair of SLA gel secondary cells connected in series. Actuator power cut-off, processor reset and power cycling, and total vehicle power kill switches are activated with magnetic proximity switches.

The central processor is an Octagon Systems Pentium III single-board computer running RedHat Linux v7.2, while each actuator module contains a Galil 1425 2-axis motion control processor. A Crossbow 6-axis accelerometer is used for navigation, with data collection performed by a 16 channel/12 bit 330KHz A/D converter from Eagle Technology.

Each of the separate housings that comprise the vehicle are connected to an Ethernet LAN with a star-shaped topology centered on a housing containing a wireless access point and hub. The appeal of Ethernet lies in both high communication rates and the ease with which new components can be connected. The Galil motion control cards were chosen in part for their compatibility with Ethernet communication, power distribution is controlled entirely through commands to an embedded server with digital I/O capabilities (a Hello!Device 1100 from Sena Technologies.) One result of the system architecture is that any computer running a web browser, and the OEM supplied software for the motion control card, can route power to one or more foil modules and control the foil motion directly.

The traditional argument against using Ethernet in control applications is that it is not structured to deliver information at deterministic times, but this is not a concern here. The microsecond timing required for the foil to accurately follow a predetermined motion path is dealt with at the actuator level in the motion control card, which is directly connected to the motor encoders. The higher level commands from the central processor must update only on the order of a fraction of foil oscillation period. The extremely low probability of packet delays over 10ms on a small, quiet local area network (LAN) is inconsequential in comparison to a minimum foil motion period on the order of 0.5-1.0s.

### C. Primary Vehicle Layout Options

The two primary vehicle layouts envisioned for the vehicle involve four foils, placed so as to take advantage of port-starboard and top-bottom symmetry. The first consists of 2 pairs of foils placed port-starboard along the median line, at bow and stern, similar to a sea turtle, as drawn in two views in Figure 3. (This configuration additionally results in fore-aft symmetry.) The second option shifts one pair of the foils $90^{\circ}$ about the vehicle primary axis, so that they are oriented up-down, a configuration not unlike that adopted by the boxfish.

The primary advantage of maximizing symmetries is the resulting simplification of the control problem and increase in open loop stability of the vehicle. The motion of the foils can be properly phased with respect to one another so as to cancel the unwanted cyclic forces that oscillating foils generally produce perpendicular to the desire impulse.

Initially, the vehicle is being assembled in the sea turtle arrangement. Maximum dimensions without foils are 2m x 0.5m x 0.5m, while the foils protrude 0.4m from each side, with 0.1m average chord. All foils have a $180^{\circ}$ range of motion in roll, and unrestricted motion in pitch. As seen in Figure 4, the actuators are mounted to an erector set style aluminum spine which measures 5cm x 10cm with a rectangular cross section. All other vehicle components, including battery and electronics housings and foam for buoyancy will be mounted directly to the same spine.

## IV. Actuator Testing

The first and second iterations of foil modules designed for the vehicle were instrumented and tested in the MIT Propeller Research Facility and the MIT Ship Model Testing Tank, respectively. Measurements were made of thrust forces, lift forces, and power consumption.

The initial goal of the testing program was to assess the likely performance of the vehicle in three specific instances: high speed cruising, transient maneuvering at speed, and hovering or station-keeping. Going forward, the availability of two instrumented actuators will allow for detailed testing of foil kinematics concurrent with testing of higher level control strategies using the vehicle itself.

### A. Kinematics

The large displacement flapping motion of the wing is referred to as the roll motion. The twisting or feathering of the wing is referred to as the pitch motion. The basic motion tested involved sinusoidal roll and pitch motions, often referred to as 'simple harmonic' foil kinematics.

The roll position of the foil is defined as,

$$\phi(t) = \phi_0 \sin(\omega t) + \phi_{bias} \tag{1}$$

where $\phi_0$ is the roll amplitude in radians and $\omega$ is the frequency of the foil motion in radians per second. $\phi_{bias}$ is a static roll bias used to change the mean roll position of the foil. For the purpose of testing with a single foil, $\phi_{bias}$ is arbitrary, but when multiple foils are in use on a vehicle, the absolute and relative values of $\phi_{bias}$ for the different foils comes into play as part of any control strategy.

The pitch position of the foil is defined as,

$$\theta(t) = \theta_0 \sin(\omega t + \psi) + \theta_{bias} \tag{2}$$

where $\theta_0$ is the pitch amplitude in radians and $\psi$ is the phase angle between pitch and roll in radians. $\theta_{bias}$ is a static pitch bias used for maneuvering. The phase angle, $\psi$, for all experiments described herein, is $\frac{\pi}{2}$ and we can therefore write $\theta(t)$ as,

$$\theta(t) = \theta_0 \cos(\omega t) + \theta_{bias} \tag{3}$$

For heaving and pitching foils, the motion is non-dimensionalized using three parameters: Strouhal number ($St$), maximum angle of attack ($\alpha_{max}$), and heave amplitude to chord ratio. The corresponding parameters in rolling and pitching motion for a flapping foil are the $St$ and $\alpha_{max}$ as calculated at a location $70\%$ of the distance from the root of the foil to the tip. The distance to this point from the axis of roll rotation is denoted by $r_{0.7}$. The ratio of the arc length at $r_{0.7}$ to the chord, denoted as $\frac{h_{0.7}}{c}$ replaces the heave amplitude to chord ratio.

Now for three dimensional kinematics we can express the angle of attack at $r_{0.7}$ as,

$$\alpha(t) = -\arctan\left(\frac{\omega r_{0.7}\phi_0 \cos(\omega t)}{U}\right) + \theta_0 \cos(\omega t) + \theta_{bias} \tag{4}$$

For three dimensional kinematics, the Strouhal number is defined,

$$St = \frac{2 r_{0.7} \phi_0 f}{U} \tag{5}$$

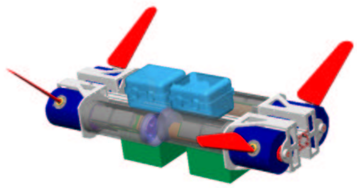

(a)

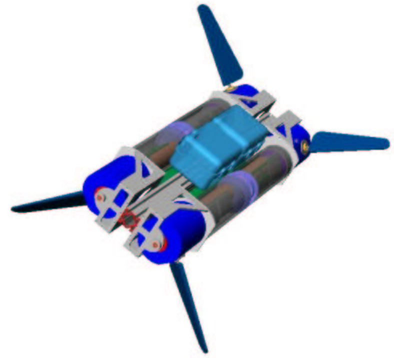

(b)

Fig. 3. Two Views of Sea Turtle Vehicle Layout

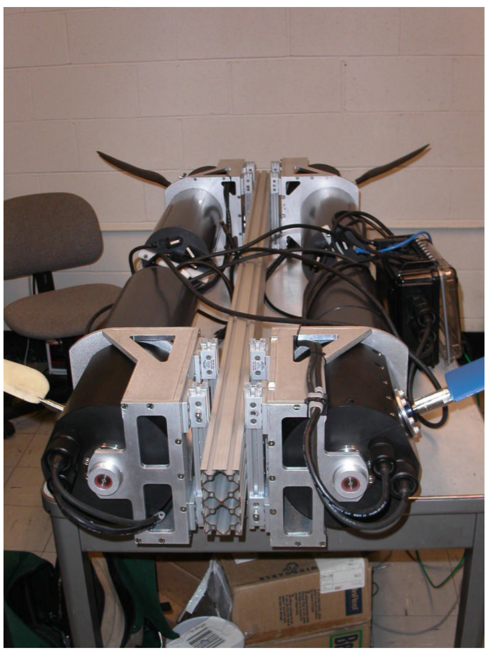

(a) Actuators mounted on frame

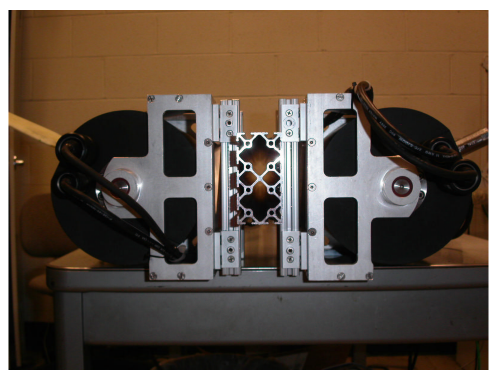

(b) Frame spine detail

Fig. 4. Frame and Actuator Assembly

The Strouhal number can be thought of as a measure of the aggressiveness of the flapping motion with respect to the incoming flow speed. Maintaining the same $St$ while increasing the flow speed requires an increase in flapping frequency, amplitude or both. The factor of two results in scaling as a function of approximate wake width, which emphasizes the relationship between $St$ and vortex shedding patterns in the foil wake.

### B. Water Tunnel Test Results

The prototype of the initial foil module design module was mounted under a six-axis dynamometer in the MIT water tunnel. The design was deemed unlikely to succeed on the vehicle itself, primarily due to the limited range of motion on the roll axis ($\pm 15°$) However, the size of the tunnel cross-section imposed an even greater restriction on foil motion for any foil of reasonable size, and so the module design problems did not limit the usefulness in testing. Details of the tunnel actuator construction and experimental apparatus can be found in [10].

Along with extensive testing of pure thrust producing modes across a range of $St$ number and $\alpha_{max}$ with flow speeds between 0.4 and 1.0 m/s, the production of maneuvering forces, i.e. forces perpendicular to the fluid flow, was investigated. The maneuvering forces were generated by adding constant bias, $\beta$ to the foil pitch angle throughout the entire propulsive stroke.

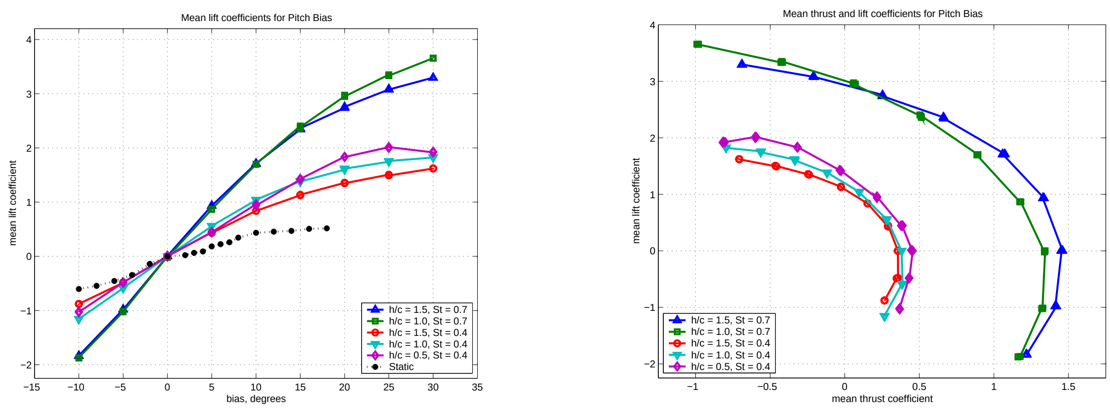


(a) mean $C_T$ v. pitch bias $\theta_{bias}$

(b) mean $C_L v.C_T$

Fig. 5. Effect of Pitch Bias on $C_L$ and $C_T$

The experiments were performed at 5 points in the sample space of Strouhal number and $\alpha_{max}$ where relatively high thrust coefficients were observed. Bias angles from $-10°$ up to $40°$ in $5°$ increments were tested at $St$ of 0.4 and 0.7 and $\frac{h_{0.7}}{c}$ values of 1.0 and 1.5. Bias angles from $-10°$ up to $30°$ were tested at $St = 0.4$ and $\frac{h_{0.7}}{c} = 0.5$. $\alpha_{max}$ for all tests was held at $40°$. Non-dimensional lift and thrust coefficients $C_L$ and $C_T$ were calculated as follows,

$$C_T = \frac{T}{\frac{1}{2}\rho U^2 A_{foil}} \tag{6}$$

$$C_L = \frac{L}{\frac{1}{2}\rho U^2 A_{foil}} \tag{7}$$

where $T$ and $L$ are the thrust and lift force, $\rho$ is the fluid density, $U$ is the flow velocity and $A_{foil}$ is the foil area.

In each case, as shown in Figure 5(a), this relatively simple pitch bias strategy resulted in a near linear relationship between lift coefficient and bias angle. A similar relationship was also found in experiments with heaving and pitching foils in the MIT testing tank [9]. Much higher lift coefficients were available in this manner than with the foil acting as a traditional, non-flapping control surface, with mean lift coefficients over 3 recorded in two cases, at $\theta_{bias}$ of $25°$ and $30°$, in contrast to a maximum lift coefficient of 0.5 before stall for the static foil.

Figure 5(b) plots the lift coefficient against the drag coefficient for each of the five sets of kinematics. The effect of higher amplitudes is seen to be much less significant than the Strouhal number in determining the location and shape of the curve. Note that maximum angle of attack is held constant throughout.

The implications for a vehicle utilizing flapping foils are the primary focus of this paper; for a more detailed discussion of the tests, including flow visualization results, see [10].

### C. Towtank Testing Results

One of the four actuators constructed for use on the vehicle was mounted to the Model Testing Tank towing carriage below a two axis dynamometer with the foil submerged (Figure 6). Testing was performed across a 4-dimensional test matrix, varying $St$, $\alpha_{max}$, $\phi_\circ$ and foil aspect ratio. The details of the experimental apparatus and the complete experimental results can be found in [11].

Figure 7 consists of plots of $C_T$ developed as a function of the non-dimensional parameters at three different values of $\phi_\circ$ to demonstrate the insensitivity of the developed thrust coefficient to the amplitude of the roll motion at any given Strouhal number and $\alpha_{max}$. The plots represent data from experiments using a foil with a span of 40cm and constant chord of 10cm, with roll angles of $20°$, $40°$ and $60°$. There is little to distinguish between the results other than the increased operational range of the actuator, in terms of the non-dimensional coefficients, when the roll amplitude is increased to $60°$. Note that for the $60°$ roll angle, thrust coefficients between 0 and 7 are available to the actuator. All of the towed experiments were performed at a towing velocity of 0.5m/s.

### D. Practical Design Tools

Plots of forces normalized by foil area and flow speed theoretically indicate how much force a foil of a given size can generate at any flow speed. However, there is an implicit assumption that the mechanism driving the foil is capable of delivering the power required regardless of the speed. In other words, while the fundamental physics underlying the efficiency and thrust development of flapping foils is illuminated by the normalization, the process hides the specific performance limits of the actuator under test.

With this caveat in mind, the region encompassed by the far right hand curve in Figure 5(b) can be interpreted as the zone of (normalized) force vectors that are known to be available to the given actuator and foil pair while the vehicle is cruising at the test speed. Even without testing the actuator to its absolute limit, it is clear that powerful turning forces can be generated while braking or thrusting. (Testing with 2-D foils suggests that pure braking forces are also available simply by changing the phasing of the pitching and heaving motions [8].)

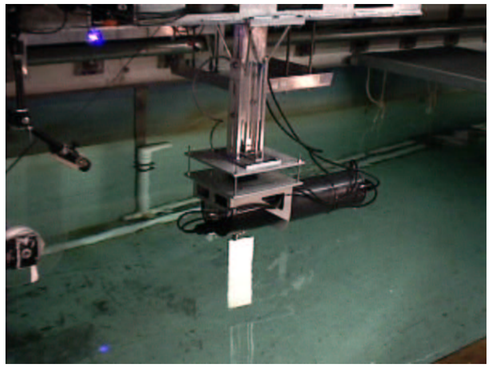

Fig. 6. Towtank Actuator Test Apparatus

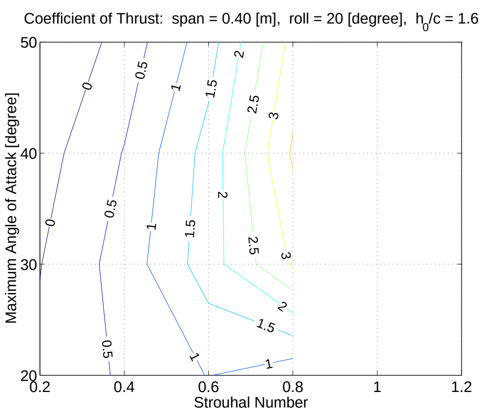


(a) 20° roll amplitude

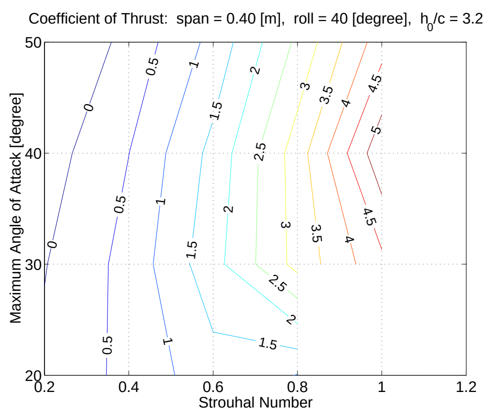


(b) 40° roll amplitude

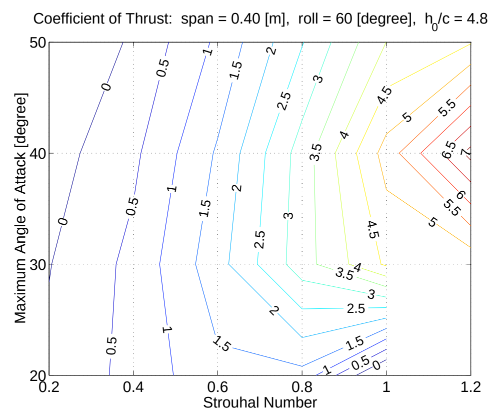


(c) 60° roll amplitude

Fig. 7. Contours of Thrust Coefficient, Roll Angle [20° 40 60]

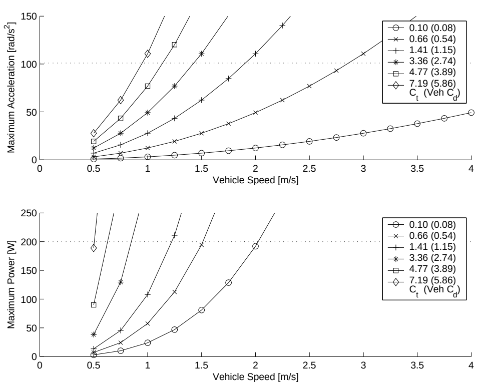


(a) Power and acceleration limits

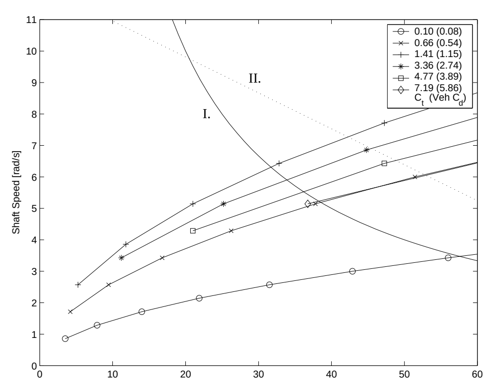


(b) Torque-speed requirements with flow speed increase

Fig. 8. Estimation of Vehicle Speed Limits with Varying $C_D$

In reality, on a normalized force plot, the attainable region will shrink as the flow speed increases because of actuator limitations. To make useful predictions for real actuator performance, a number of assumptions need to be made:

- The distance, $r_{eff}$, from the roll axis to the effective center of force on the foil is a function of Strouhal number and $\alpha_{max}$.
- Maximum lift is experienced at the maximum roll angular velocity.
- Maximum roll motor torque coincides either with maximum lift or maximum foil acceleration.
- Added mass of water in rotation about the roll axis is much smaller than the rotational inertia of the moving parts of the actuator.

The motor torque requirement at the moment of maximum $C_L$ should scale with the lift force, $L$, when the Strouhal number, $\alpha_{max}$ and $\theta_{max}$ are unchanged,

$$\tau_{max} = L_{max} r_{eff} \tag{8}$$

Hence, the roll motor torque requirement at the moment of maximum lift scales with $U^2$,

$$L_{max} = \frac{1}{2}\rho U^2 A_{foil} C_{Lmax} \sim U^2 \tag{9}$$

By the assumptions above, the roll motor speed requirements peak at this moment as well,

$$\dot{\phi} = \phi_{\circ}\omega \cos \omega t \tag{10}$$

$$\dot{\phi}_{max} = \phi_{\circ}\omega \tag{11}$$

From (5),

$$\phi_{\circ}\omega = \frac{U \cdot St}{r_{0.7}\pi} \sim U \tag{12}$$

Hence shaft speed scales with flow velocity as well. Since output power for the motor is calculated as,

$$P = \tau\omega \sim U^3 \tag{13}$$

it follows that power output required at the moment of maximum lift scales with the flow velocity cubed when $St$ and $\alpha_{max}$ are held constant.

The rotational inertia must be accounted for at the point of maximum foil roll acceleration, where,

$$\ddot{\phi} = -\phi_{\circ}\omega^2 \sin \omega t \tag{14}$$

$$|\ddot{\phi}_{max}| = \phi_{\circ}\omega^2 \tag{15}$$

Ignoring the added mass of the fluid, which we do not know as a function of $St$ and $\alpha_{max}$, we find that the torque required to overcome the rotational inertia in the roll scales linearly with the roll amplitude and with the square of the frequency.

The discussion of actuator limits here has focused on the roll actuation, as it is clear from experiments with the current module that the pitch motor is grossly overpowered with respect to the roll motor for the simple harmonic kinematics described above. (The pitch motor was sized to allow force vectoring using high frequency pitching with no roll motion, a technique which has not yet been investigated with this actuator.)

It is now possible to make a quantitative estimate of the actual velocity limit for a vehicle using four of the existing foil modules, with 0.40m x 0.10m foils. In both configurations described above, all four foils are oriented with the foil thrust direction directly forward in the vehicle body frame. Defining a drag coefficient for the vehicle based on the vehicle projected frontal area, $A_{vehicle}$,

$$C_D = \frac{D}{\frac{1}{2}\rho U^2 A_{vehicle}} \tag{16}$$

we find that at every attainable speed, the total thrust force produced by the foils must overcome the body drag,

$$T_{tot} = C_T \cdot (\frac{1}{2}\rho U^2) \cdot A_{foils} = C_D \cdot (\frac{1}{2}\rho U^2) \cdot A_{vehicle} \tag{17}$$

$$C_T = C_D \frac{A_{vehicle}}{A_{foils}} \tag{18}$$

Hence, the maximum speed of the vehicle, as a function of the drag coefficient of the vehicle, is the maximum speed at which a foil actuator can produce the corresponding $C_T$, which is a function of the ratio of the surface area of the foil to the frontal area of the vehicle.

Figure 8(a) indicates how the inertial and the hydrodynamic limits on the actuator roll motor limit the maximum speed of the vehicle. The inertial limit is manifested as a limit on the maximum acceleration of the foil, which is set to a conservative value of $101\frac{rad}{s^2}$ based on the maximum acceleration achieved by the actuator during tests with the 0.40m foil in water. The hydrodynamic limit is a function of the power limitations of the actuator, which in this case stems from current limiting the roll motor amplifier to 12A at 24V, and the manufacturer's estimate of $75\%$ efficiency across the motor's two stage planetary gear head.

The power and acceleration requirements are extrapolated from 6 data points, representing 6 different sets of foil kinematics operating at a flow speed of 0.5m/s. These kinematics were considered desirable because of their relatively low maximum current draw as a function of thrust coefficient, as experimentally demonstrated in the Towing Tank. The foil thrust coefficients range from 0.10 to 7.19, which correspond to vehicle drag coefficients of 0.08 to 5.86 given a ratio of foil area to vehicle frontal are of 0.8. The figures indicate that regardless of the vehicle drag coefficient, the primary limitation on the vehicle maximum speed is the power required to drive the foil at maximum velocity, which scales with $U^3$, rather than the torque required to accelerate the foil apparatus, which scales with $U^2$. Figure 8(b) plots the paths of the motor operation point with increasing speed on a torque-speed plot to indicate how the maximum power limit is approached when operating at each of the 6 selected thrust coefficients, where II is the nominal motor torque-speed curve at 24V, and I represents maximum power output of 201W. Each point to

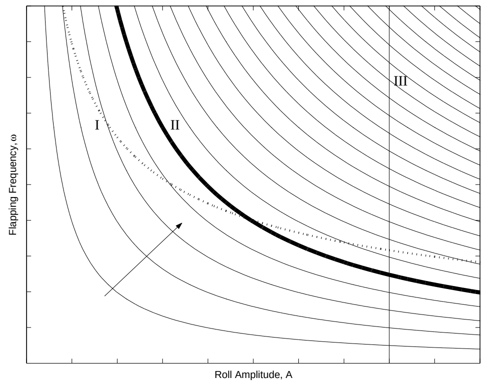


Fig. 9. Shape of Actuator Hovering Limits

the right along a curve represents a vehicle speed increase of 0.25m/s

For an extremely streamlined vehicle, a drag coefficient of 0.1 is attainable with difficulty, which would yield a vehicle maximum speed of greater than 2m/s. Without a streamlined fairing, a drag coefficient between 0.8 and 1.4 is more appropriate, from [12] based on the drag on a blunt cylinder with aspect ratio $\frac{l}{d} = 4$, indicating a maximum speed under 1m/s.

### *E. Control Implications*

From a vehicle control perspective, the linear relationship between bias angle and lift force is appealing, as it suggests that control strategies used with traditional control surfaces can be extended to include flapping foils.

Figure 5(b) demonstrates that a foil should be able to generate maneuvering forces perpendicular to the vehicle motion while it is being used to propel the vehicle. The shape of the curves about the zero mean lift point in each case indicates that for small bias angles (less than $5°$) significant lift can be developed with relatively slight drop in thrust. The weak coupling between thrust and lift generation for small pitch bias for a given operating point should allow for decoupling of speed and pitch control in a vehicle being controlled to constant forward speed. In the sea-turtle configuration, there is the option to use either one or both pairs of foils in concert to generate pitch moments. In the boxfish orientation, yaw can also be actuated by using pitch bias on the up-down oriented fins.

For speed control, accurate measurement of flow speed will be necessary to ensure that effective kinematics are chosen for the foils. Once a steady-state speed has been achieved, maintaining that speed may be as straightforward as a PID controller which varies the frequency of the foil motion, as the foil thrust coefficient is generally a strong function of Strouhal number. In both speed and pitch control, some higher level decisions about the relative merits of adjusting frequency and amplitude to achieve the desired Strouhal number will need to be made as well. As demonstrated in Figure 8(a), the rotational inertia of the apparatus does not limit the vehicle speed when using a consistent roll amplitude of $60°$ for cruising, indicating that lower roll amplitudes and higher frequency motions could be used to achieve the same total thrust.

The appeal of higher frequency motions is greater control bandwidth, assuming that the kinematics of the foil motion are adjusted only after complete swimming strokes. For example, reducing roll amplitude to $20°$ from $60°$ at a flow speed of 0.5m/s, assuming a desired thrust coefficient of 1.4, would increase the flapping frequency from 0.3Hz to 1Hz. Eventually, a frequency and amplitude combination would be reached at which the rotational inertia of the actuator would effectively limit the motion. (Operating in air, the actuator has briefly been driven to frequencies as high as 1.5Hz at roll amplitudes as high as $30°$.)

A similar tradeoff between bandwidth and actuator authority is likely to be found when considering zero speed maneuvers, i.e. hovering. In previous experiments in the Testing Tank with heaving and pitching foils [9], and in tests with the vehicle actuators, both the the mean thrust developed over a cycle of simple harmonic motion and the maximum current draw are primarily functions of the maximum roll angular velocity.

Assuming, then, that contours of both the roll motor power requirement and the developed thrust lie along lines of constant $\dot{\phi}_{max} \sim \phi_\circ \omega$, and recalling that the effect of actuator rotational inertia scales with $\phi_\circ \omega^2$, the limits on actuator operation at zero speed can be sketched out as in Figure 9. Curve I indicates the acceleration limit imposed by the internal rotational inertia. Curve II is the power limit, whose shape results from the assumption that motor power is a monotonically increasing function of maximum angular velocity. Curve III indicates a hard physical limit on the roll amplitude, $\phi_\circ$, which is $90°$ for this actuator.

Thrust contours increase following the arrow from the bottom left to the top right, so a level of thrust can be achieved only if the corresponding contour at some point is to the left and below each of the limit curves. By following thrust contours of increasing magnitude all the way to the point where they cross I, it becomes clear that the higher the level of thrust, the lower the maximum frequency at which it can be achieved.

## V. CONCLUSION

The testing of the foil actuators in the Testing Tank and Water Tunnel is a promising step towards the realization of the Biomimetic Flapping Foil AUV. With estimates for the vehicle performance in hand, it will be possible to determine whether the performance limits of the fully realized vehicle, when it is launched, result from the fundamental limits of the actuators themselves, or stem from other sources such as improper control strategies and foil kinematics. Going forward, the ultimate purpose of the BFFAUV is to be a platform for experimentation with control strategies, vehicle shapes, and foil properties. The current design should combine a high level of performance and robustness with real flexibility in implementing different approaches to the challenging issues ahead in the development of foil powered vehicles.

## Acknowledgment

The authors acknowledge with gratitude financial support by the MIT Sea Grant Program and the Office of Naval Research STTR Contract N0014-02-M-0219, monitored by Dr. P. Bandyopadhyay.

## References

[1] M. Triantafyllou and G. Triantafyllou, "An efficient swimming machine," *Scientific American*, vol. 272, no. 3, pp. 64–70, 1995.

[2] M. Triantafyllou, D. Yue, S. Tolkoff, A. Techet, D. Barrett, F. Hover, M. Grosenbaugh, W. McGillis, and M. Wolfgang, "Drag reduction and turbulence control in swimming fish-like bodies."

[3] D. Barrett, M. Triantafyllou, M. G. D. Yue, and M. Wolfgang, "Drag reduction in fish-like locomotion," *Journal of Fluid Mechanics*, 1999.

[4] F. Fish, "Power output and propulsive efficiency of swimming bottlenose dolphins," *Journal of Experimental Biology*, vol. 185, pp. 179–193, 1993.

[5] G. Lauder and B. Jayne, "Speed effects on midline kinematics during steady undulatory swimming of largemouth bass," *The Journal of Experimental Biology*, no. 198, pp. 585–602, 1995.

[6] J.Videler, *Fish Swimming*. London: Chapman and Hall, 1992.

[7] J. Anderson, "Vorticity control for efficient propulsion," PhD Thesis in Oceanographic Engineering, Massachusetts Institute of Technology, MA, February 1996.

[8] D. Read, "Oscillating foils for propulsion and maneuvering of ships and underwater vehicles," Master of Science in Naval Architecture and Marine Engineering, Massachusetts Institute of Technology, MA, February 1999.

[9] O. Haugsdal, "Motion control of oscillating foils for steady propulsion and starting maneuvers," Master's Thesis, Massachusetts Institute of Technology, MA, 2000.

[10] M. Flores, "Flapping motion of a three dimensional foil for propulsion and maneuvering of underwater vehicles," Master of Science in Ocean Engineering, Massachusetts Institute of Technology, MA, May 2003.

[11] V. Polidoro, "Flapping foil propulsion for cruising and hovering autonomous underwater vehicles," Master of Science in Ocean Engineering, Massachusetts Institute of Technology, MA, May 2003.

[12] S. Hoerner, *Fluid-Dynamic Drag*. Vancouver, Washington: Hoerner Fluid Dynamics, 1965.